ELSEVIER

Resistive (dry?) lower crust in an active orogen, Nanga Parbat, northern Pakistan

Stephen K. Park [a],*, Randall L. Mackie [b]

[a] *Institute of Geophysics and Planetary Physics, University of California, Riverside, CA 92521, USA*
[b] *GSY-USA, Inc., 2261 Market St, Ste 643, San Francisco, CA 94114, USA*

Abstract

Conductivity models beneath the Nanga Parbat Haramosh Massif (NPHM) derived from magnetotelluric soundings reveal that there is no widespread, interconnected, conductive aqueous fluid to minimum depths of 40 km below sea level. Given the continuing tectonic denudation, young granitic and migmatitic bodies indicating partial melt at shallow crustal depths, and active seismicity, this result is surprising in light of similar studies in active tectonic regimes elsewhere. Away from the NPHM, models reveal the usual conductive lower crust. We propose that deep magmatic and metamorphic fluids are produced beneath NPHM in isolated zones but that the active deformation permits their escape through the brittle–ductile transition. A magnetotelluric survey in an area as complicated as Nanga Parbat required the development of methodologies for utilizing standard two-dimensional inversions in a three-dimensional environment. We show here how to identify which parts of the magnetotelluric responses are adequately represented with two-dimensional approximations. Unlike previous efforts, we do not attempt to create a set of generic rules that may be applicable to all geologic environments. Instead, a procedure is outlined that can be tailored to each interpretation. One important result of this work is that magnetotelluric data along a profile can be used to constrain structure off the ends of the profile. © 2000 Elsevier Science B.V. All rights reserved.

Keywords: Himalayas; magnetotelluric methods; Nanga Parbat; Pakistan

1. Introduction

Nanga Parbat in the Himalaya of northern Pakistan (Fig. 1) rises over 8000 m above sea level and is an active site of crustal reworking including metamorphism and partial melting. Paleobarometry and ages of gneisses and migmatites at the core of the massif have led to the inference that the mountain has been exhumed at rates of 3–6 mm/year over the past 3 Ma (e.g. Zeitler, 1985;

Zeitler et al., 1993). With the middle crust currently exposed at the surface and geothermal activity in the region indicating that crustal reworking is still active, Nanga Parbat provides a unique glimpse into the processes that rework continental crust.

The high peak of Nanga Parbat lies in a north–south-oriented antiform called the Nanga Parbat–Haramosh Massif (NPHM) created by collision between Kohistan and the Indian plate along the Main Mantle Thrust (MMT). Lying at the western syntaxis of the collision between India and Asia, this antiform has been the site of extensive exhumation in the past 10 Ma that has completely removed

* Corresponding author. Tel.: +1-909-787-4501;
fax: +1-909-787-4509.
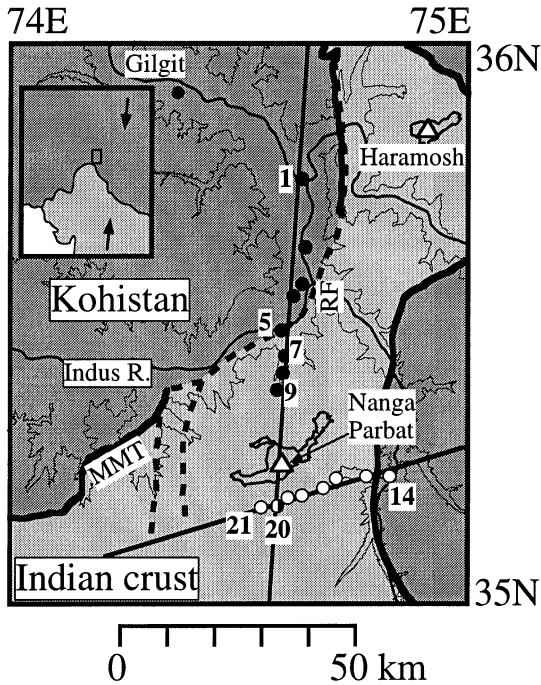*E-mail address:* magneto@ucrmt.ucr.edu (S.K. Park)

Fig. 1. Location map showing relationship between MT soundings (black dots for those on N–S transect and white dots for those on E–W transect) and geologic structure. The Main Mantle Thrust (MMT; solid line) and the Raikot Fault (RF; dashed line) separates the underlying Indian crust from overlying Kohistan. Elevation contours of 3000 m (light line) and 6000 m (heavy line) are shown, as is the Indus River. Site numbers between 1 and 5, 7 and 9, and 14 and 21 are sequential and not labeled. Site 20 is common to both MT transects, which are shown with black lines passing through sites.
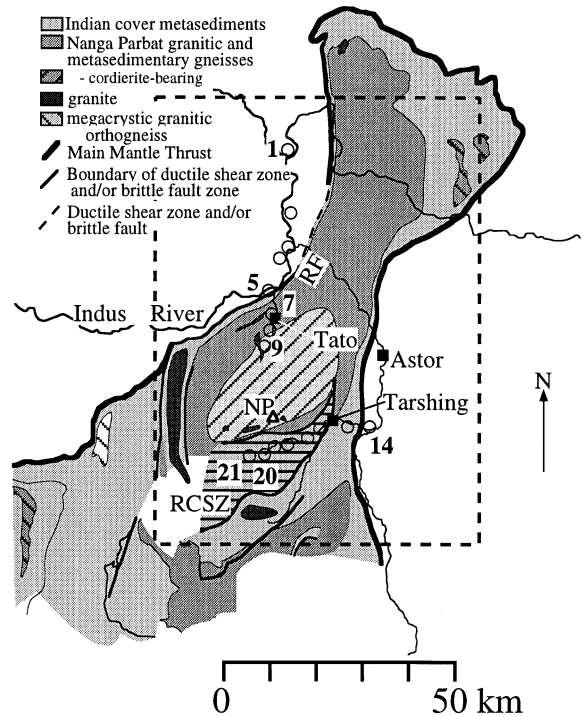

Fig. 2. Geologic map generalized from Schneider et al. (1999). Only geology in the Nanga Parbat–Haramosh Massif (NPHM) is shown; igneous and high-grade metamorphic rocks of Kohistan are left out. MT sites are all shown as open circles. The villages of Tato, Astor, and Tarshing are shown, and sites 15–21 lie in the Rupal Valley mentioned in the text. Symbols used here are: NP, Nanga Parbat; RF, Raikot fault; RCSZ, Rupal Chichi shear zone. The area of Fig. 5 lies within the dashed line. The central cordierite-bearing granitic and metasedimentary gneisses south of Tato and north of Nanga Parbat delineates the region of most rapid exhumation.

the overlying high-grade metamorphic and plutonic rocks of Kohistan and exposed the underlying Indian crust (Fig. 1). While the entire NPHM has experienced this rapid uplift, the region north of Nanga Parbat has experienced the most dramatic exhumation. This region, bordered on the north by the Indus River (Fig. 2), has cooling ages between 1 and 3 Ma from biotites in cordierite-bearing granitic and metasedimentary gneisses (Schneider et al., 1999). The presence of cordierite indicates metamorphism at depths of 15 ± 8 km and temperatures of 600°C prior to exhumation. Isolated granitic plutons (Fig. 2) and leucogranite dikes are also found in this region and indicate that partial melting is occurring at depth (Schneider et al., 1999). Similar ages between the

granulite grade metamorphic rocks and the leucogranitic dikes lead to the conclusion that prograde metamorphism and melting are contemporaneous (Smith et al., 1992).

Because the NPHM is an ideal laboratory for observing the evolution of continental crust via crustal reworking, it was the focus of a multidisciplinary Continental Dynamics study funded by the National Science Foundation. A magnetotelluric (MT) survey was included as part of this research in order to determine the extent and distribution of aqueous fluids and partial melt in the crust. In particular, we did not know whether the granitic melts were produced by decompression melting of

dry continental crust as exhumation proceeded or by fluxing of the crust with fluids from dewatering reactions in the adjacent crust or underlying subducted plate.

Aqueous brines are the source of prominent conductivity anomalies in many MT studies. Thus, independent information about the type and state of these fluids is crucial to an interpretation. Nanga Parbat has abundant evidence of aqueous fluids in the rapidly exhuming region. Hot springs are common, especially along the Raikot fault and near Tato (which means 'hot' in the local dialect). Studies of fluid inclusions from quartz veins in the leucogranites indicate that aqueous inclusions are the most common, although CO_2 inclusions are also found (Craw et al., 1994). The aqueous fluid inclusions homogenize to vapor at temperatures of 320–410°C, indicating formation in a dry steam geothermal system in the upper 5 km (Craw et al., 1994, 1997). Craw et al. (1994) concluded that the fluid in the inclusions came primarily from circulation of meteoric water into the hot rocks. Based on the temperatures and depths, they estimated a geothermal gradient of 100°C/km. A later study showed that the aqueous inclusions contained 5 wt% NaCl and that there were deeper fluids perhaps related to metamorphism (Craw et al., 1997). However, these fluids were different from typical granulite facies metamorphic fluids or from crystallizing magmas. With these studies, we can conclude that aqueous fluids are likely to be a significant source of shallow (and perhaps deep) crustal conductivity at Nanga Parbat.

Surprisingly, our study has revealed that the crust is resistive to depths of more than 60 km below sea level (bsl) beneath the youngest, most rapidly exhumed crust. We will show that conductive zones indicative of interconnected brines lie to the south of Nanga Parbat and along the Raikot fault. Coupled with seismic tomography, our results indicate that water-undersaturated decompression melting is the most likely source of the granitic melts.

2. Magnetotelluric method

Magnetotelluric studies are a relatively recent addition to tectonic investigations and have been used to map the distributions of fluids in tectonically active regions. Vector electric and magnetic time series are acquired at individual sites and converted to tensor, frequency-dependent impedance functions (Vozoff, 1991). Tensor impedances from multiple sites, usually along a profile, are then inverted to generate a two-dimensional (2-D) cross-section of electrical resistivity. MT data are most sensitive to conductive regions, so geological interpretation usually consists of identifying the causes for high conductivity (Jones, 1992). Mafic partial melts, water-saturated silicic melts, brines and metamorphic or igneous waters, metallic solid phases, and graphite are all capable of increasing the conductivity of the crust and upper mantle (Jones, 1992). Within the mantle, brines do not wet the surfaces of ultramafic rocks (Watson and Brenan, 1987) and only basaltic melts and solid phase conduction can low the resistivity of the rocks.

An implicit assumption in the transformation of the observed impedances to a resistivity cross-section is that the profile is perpendicular to a 2-D structure. The tensor impedance is decomposed into two principal impedances (much as areal strain can be decomposed into two principal strains), each with a magnitude, phase, and direction. In the case of 2-D structures, these principal impedances are oriented parallel and perpendicular to the geological strike of the structure. The mode perpendicular to strike is called the TM mode (this is the mode oriented parallel to the plane of the cross-section), and the mode parallel to strike is the TE mode. We will use this notation for modes when discussing the 2-D resistivity cross-sections derived for the data. Decomposition of the electromagnetic equations for 2-D structure also predicts that can be a vertical magnetic field (Hz) aligned along the principal impedance parallel to the TM mode only. The transfer function relating Hz to the horizontal magnetic field is therefore included in the transformation of impedances into a resistivity cross-section.

A two-dimensional structure is clearly not present at Nanga Parbat, and one contribution of this study is a methodology to evaluate the validity of the 2-D assumption by using three-dimensional (3-D) modeling. Rather than developing a univer-

sal rule by which components of the tensor imped-ance can be interpreted with 2-D slices in a 3-D earth, we instead outline an iterative method using 2-D cross-sections and 3-D modeling for inter-pretation in this setting. Note that the methodol-ogy can be transferred to new areas, but the results presented here are specific to this area. We build on the results of Park and Mackie (1997) and discuss the N–S transect only in light of new data. Once we have a model that is consistent with the observed impedances, the robustness of portions of this model is assessed by sensitivity studies. In particular, we determine what constraints can be placed on various resistivity structures in the cross-section. The first section discusses acquisition and processing of the MT data, while the second illustrates our methodology for determining the validity of the 2-D assumption at Nanga Parbat. The third section presents the results of our sensi-tivity analysis, and the fourth section discusses the geological implications of resistive crust beneath Nanga Parbat.

3. Magnetotelluric data

The locations of MT sites were dictated largely by access in the rugged topography surrounding Nanga Parbat (Fig. 3). Most of the data acquired

Fig. 3. Looking north from Tato along the Indus River and the N–S MT transect. Note the extremely rugged terrain that con-trolled site placement.

near the high peak required transport by porters via foot. As a result, the distribution of sites was not driven by scientific targets as much as by logistics (Fig. 2). Data were acquired along two roughly linear and orthogonal transects, one of which passed through the peak itself (Fig. 1). Data were recorded at periods between 0.008 and 1024 s using EMI's MT-1 magnetotelluric system. Data were acquired simultaneously at pairs of sites so that remote referencing could be used for noise reduction. Timing between sites was provided by synchronized clocks with drifts of less than 1.0 ppb per day. While site separations of 5–10 km were possible along the Indus River and east of Tarshing where roads were available, site separations in roadless regions were typically 2–3 km and con-trolled by walking times between sites (2–3 h). This part of Pakistan has few sources of cultural noise, so primary noise sources included coil vibrations caused by flowing streams and blowing wind. Site separations of 2–3 km were sufficient to reject these sources of noise in the analysis.

Time series at sites along the E–W profile were analyzed with two different robust processing codes. Most of the data were processed with Chave et al.'s code (Chave et al., 1987), which uses rejection in the frequency domain of data segments with poor coherencies between observed and pre-dicted electric fields. Sites 16 and 17 still showed substantial scatter in the impedance estimates after robust processing with remote reference however, and Larsen et al.'s (Larsen et al., 1996) robust analysis was applied at these few sites. (Note that we will use the actual site numbering from the database in order to allow future researchers to compare their results directly to those presented here.) This latter analysis rejects outliers in both the time and frequency domains, and resulted in much smoother estimates of the MT impedance at longer periods. Comparison of results from the two processing techniques revealed that average values were very similar, but responses from Larsen et al.'s code were smoother, and errors were smaller. We conclude from this comparison that noise at these sites consisted primarily of transient em signals likely emanating from a nearby village (perhaps from livestock disturbing the lines or from portable generators).
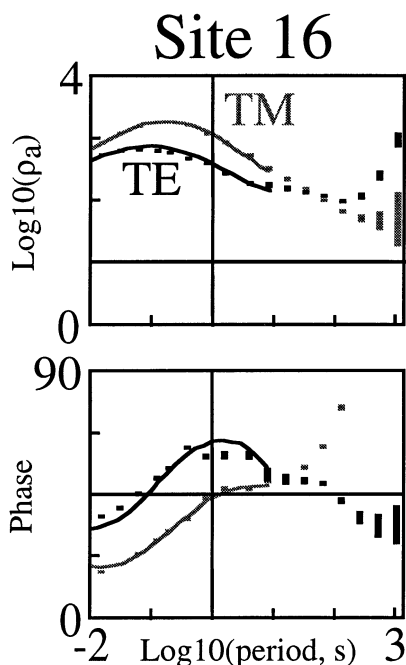
Site 16

Fig. 4. Apparent resistivity and phase sounding curves from site 16 in the shear zone on the E–W transect. Following conventions for presentation of MT data, impedance magnitudes are scaled as apparent resistivities in ohm-m and plotted on a log–log plot versus period. Impedance phases in degrees are plotted on a log-linear plot versus period in seconds. Data are shown as gray or black vertical lines with the length of lines denoting uncertainties in values, while model fits are plotted as gray or black solid lines. The extent of the model fits denotes the range of periods used in the modeling; data at periods longer than 8 s were not used in the E–W model. Modes are indicated with TE (N30W) and TM (N60E) labels. The TM response at periods longer than 10 s is not minimum phase, likely indicating competing effects from the shear zone and the conductor to the south of the E–W transect. The response at site 15 (not shown) was similar.

Distortion analysis was applied at all sites initially (Groom and Bailey, 1989), but the principal effect of this analysis was to remove static shifts only (as evidenced by removal of the high-frequency anisotropy between the two modes of the apparent resistivities). The only exceptions were at sites 7–9, where Park and Mackie (1997) found that the distortion analysis also removed significant angular distortions. Sites 15–17 also had clear distortion effects associated with local structure (Fig. 4), but these could not be corrected by the

analysis. We therefore used the distortion analysis at sites 7–9 only.

Data along the E–W transect are complicated by the presence of a shear zone crossing obliquely to the orientation of the profile (Fig. 2). Maximum apparent resistivities within the shear zone (sites 18–21) are consistently oriented at N30W. This impedance strike is parallel to orientations of Parkinson induction arrows at longer periods at these sites and others along this profile (Fig. 5). If the impedance strike and induction arrows were responding primarily to a conductive shear zone, then the induction arrows should have been perpendicular to direction of the maximum apparent resistivity. Because this was not the case, both quantities must be influenced primarily by another structure(s). As is discussed below, the impedance strikes and induction arrows are responses to a conductive zone to the south of the E–W profile.

An orientation of N30W is approximately perpendicular to the local strike of the Rupal Valley and parallel to the plane of a profile passing through these sites (Fig. 1). The use of a 2-D model along this profile usually entails rotation of the MT impedances into directions parallel and perpendicular to the profile. At the boundaries and just outside the shear zone (sites 14–16) however, the geoelectrical strike is oriented north (or parallel to the local strike of the shear zone and the MMT boundary — Fig. 5). In a region with multiple structures oriented both transverse and obliquely to the profile, we preferred to use the local geoelectrical strike rather than a single value at all sites. For example, rotation of site 16 (Fig. 4) to an orientation of N30W mixed the modes parallel and perpendicular to the shear zone so that two almost identical responses resulted. Use of the local geoelectrical strike captured the essential electrical behavior of the shear zone as its local azimuth changed.

A similar situation exists on the N–S transect where it crosses the locally NE-trending Raikot fault zone (Figs. 2 and 5). Strikes at sites 5–7 are oriented N45W, rather than N–S as seen elsewhere along the profile. While the fault appears as a single, well-defined boundary on the map, field observations reveal multiple, small faults in this region. Indeed, the village of Tato (Fig. 2) has hot
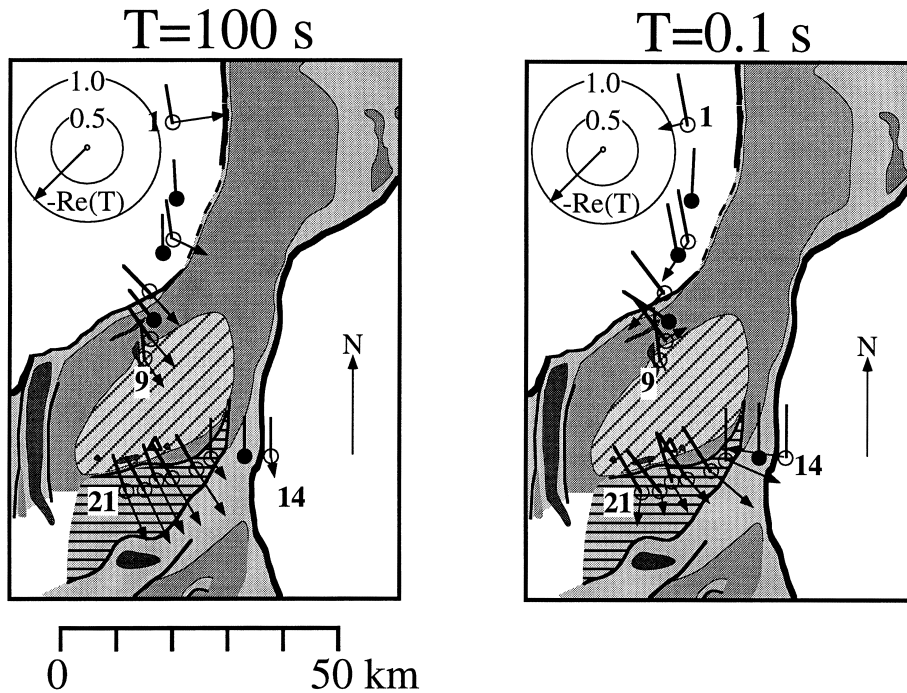
T=100 s   T=0.1 s

Fig. 5. Simplified geologic map from Fig. 2 with impedance strikes (heavy black lines at each site) and Hz transfer functions (lighter black lines with arrows) shown. Data are plotted for periods of 0.1 and 100 s. The tipper transfer function plotted is the negative of the real component, which conventionally points towards good conductors (Parkinson, 1962). Site locations are indicated with open dots, where Hz was recorded and black dots where Hz was not recorded. Note the consistent orientation of approximately SE for most 100 s transfer functions on the massif, indicating a good conductor to the south of the E–W transect in Rupal Valley.

springs emanating from one of these faults. Rotation of the modes at these sites by 45° (i.e. to the north) mixed modes parallel and perpendicular to the fault in such a manner as to yield identical responses for the N–S and E–W modes. This clearly did not capture the essential electrical behavior of the fault. We therefore chose to use a N–S strike for all sites except for sites 5–7 (where N45W was used). In both transects, modes parallel and perpendicular to the local geoelectrical strike were chosen for the TM and TE modes, respectively.

Static shifts were assigned to sites after rotation to chosen geoelectrical strikes (N–S or N45W for the N–S transect, following Park and Mackie (1997), and N30W or north for the E–W transect; see Fig. 5). These static shifts are provided in Table 1. Geometric means of the short period responses at sites on similar geologic materials were used to set these static shifts; Hirasuna and

Park (1993) showed that this worked as well in mountainous terrain as did independent measures from transient electromagnetic soundings.

4. Two-dimensional profiles in a three-dimensional setting

Three-dimensional inversion is not yet commonly available, and it is unclear whether it would be useful with such a sparse data set as this one. Trial-and-error forward modeling with 3-D models, as tried by Park and Torres-Verdin (1988) or Mackie et al. (1996), is similarly unsatisfying and time-consuming. We instead used 2-D inversion of data along the N–S and E–W transects, judiciously choosing to invert only those data that are less affected by structure parallel to the profiles. These data will be identified through the use of 2-D and 3-D models. This is an iterative process

Table 1
Static shifts and distortion corrections

Site	Azimuth	Twist	Shear	Multiplicative static shift factors	
				(N–S or NW)	(E–W or NE)
1	N–S	0	0	1	1
2	N–S	0	0	1	1
3	N–S	0	0	1	0.46
4	N–S	0	0	1	1
5	N45W	10	0	1	1
7	N45W	0	20	1	1.87
8	N45W	−40	−15	1.62	0.59
9	N–S	0	−30	1	1
14	N–S	0	0	1.21	0.86
15	N–S	0	0	1	1
16	N–S	0	0	1.32	1
17	N30W	0	0	0.35	1
18	N30W	0	0	1	0.62
19	N30W	0	0	1	0.58
20	N30W	0	0	1	1
21	N30W	0	0	0.62	2.21

because these 2-D and 3-D models are derived from the data, which we then test for the effects of 3-D structure. The results are models of the N–S and E–W profiles, which are consistent with a composite 3-D model of the region.

An additional complication with two orthogonal 2-D profiles is that the TE mode for one is the TM mode for another, and this will lead to confusion regarding references to these modes. Throughout this paper, we will adopt the convention of referring to TE and TM modes based on the profile orientation. We will also put the compass orientation in parentheses after the TE or TM label, so that the orientation is perfectly clear. Where the profiles cross at site 20, the N30W mode will be the TM mode for the N–S profile and will be designated as TM (N30W). That same mode will be the TE mode for the E–W profile and will be designated as TE (N30W). The mode designation is consistent with terminology for 2-D models, while the compass direction will identify uniquely which component of the impedance tensor is used.

Park and Mackie (1997) showed that data along the N–S transect were affected by shallow sediments along the Indus River valley, but that valid 2-D models of the TM (N–S) mode of the impedance

could be derived. They also showed that the TE (E–W) mode of the impedance at sites 7, 8, and 9 could be included in those 2-D models because it was not affected by the Indus River valley (Fig. 6). This conclusion was reached by comparing a 3-D model of the Indus River sediments to a corresponding 2-D model. Truncation of the sediments to the east and west of the N–S profile severely distorted the TE (E–W) mode (Fig. 6). We have now added an additional site (site 20) to their original profile but have to assess the limits of the 2-D approximation in the Rupal Valley. In addition, results presented here for the N–S transect reveal that a large conductive body lies south of the E–W transect. We must assess the impact of that body on a 2-D approximation for data along the E–W transect. Clearly, there is no apriori way in a 2-D analysis of including the influence of conductive bodies oriented parallel to profile strike. We will therefore make some assumptions about the limits of the 2-D approximation and then demonstrate that those assumptions are valid.

Our strategy is to begin with the 2-D model for the N–S transect and then show how the structure north or south of the E–W profile will affect the data used on the N–S profile (Fig. 7). Inversion of the data along the E–W profile that can accurately
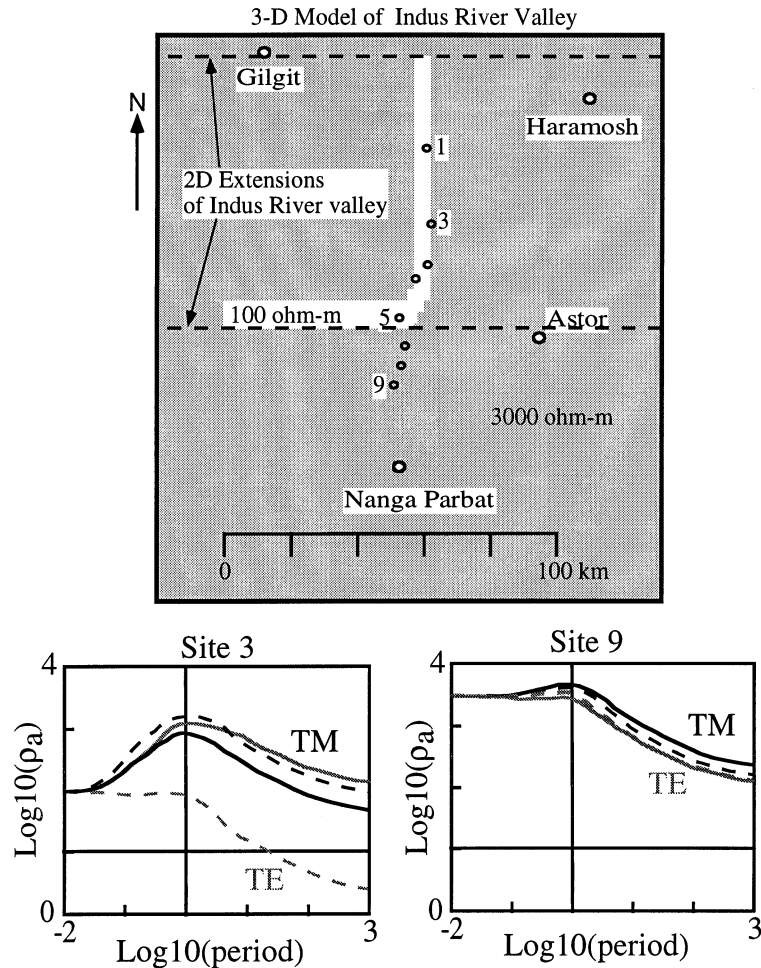
3-D Model of Indus River Valley

Fig. 6. 3-D model of the upper 700 m of the crust showing the sediments along the Indus River valley. For this test, the model was 1-D below 700 m. Responses at sites 3 and 9 were computed using Mackie et al.'s finite difference code (Mackie et al., 1996). The dashed lines are for the model shown, and the solid lines are computed by extending the sediments to the east and west in accordance with a 2-D structure crossed by the N–S profile. Note that the TM (N–S) curves are within a factor of two at site 3, but that the TE (E–W) responses differ by a factor of 100. Both sets of responses are similar at site 9, showing that neither mode is affected significantly by the Indus River sediments.

be represented with a 2-D model is then performed. The effects of N–S-oriented conductive bodies from this inversion on data along the N–S transect are then estimated. If necessary, the inversion along the N–S transect is then recomputed using only those data that can be represented by 2-D models. The tests discussed above will be based on 2-D modeling, but we will also show that a 3-D composite model of the cross-sections from the N–S and E–W transects confirm our conclusions based on the 2-D

approximations. Once we have verified that we have valid 2-D models, we then examine bounds on the structures through a sensitivity analysis similar to that of Park et al. (1996).

4.1. N–S transect

We use the TM (N–S) modes from sites 1–9 and the TE (E–W) modes from sites 7–9, in accordance with our earlier study (Park and
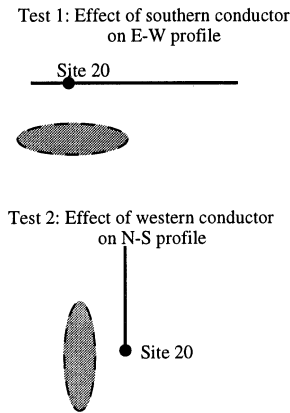
Fig. 7. Schematic diagram showing tests of 2-D assumption for N–S and E–W transects.
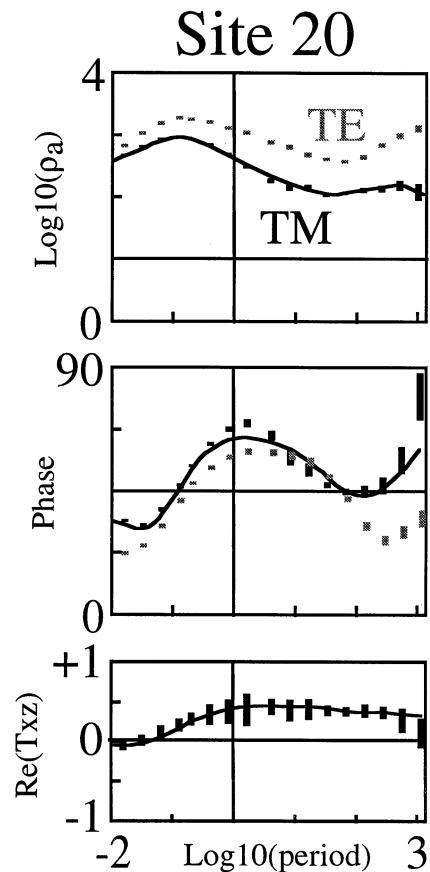

Fig. 8. Data and model fits at site 20 for N–S transect. Conventions for plotting are explained in Fig. 4. Note that only the TM (N30W) mode was fit with this model because we will show below that the TE (N60E) mode was affected by structure to the west of the transect. The Hz transfer function and its model fit are also shown. Txz is the transfer function in the N30W direction at this site (approximately parallel to the transect and perpendicular to the 2-D structure).

Mackie, 1997). We must assess which modes to use from site 20, however. Topography and surface geology shows that site 20 lies in a region with structures oriented approximately perpendicular to the strike of the N–S profile (Figs. 1 and 2). The geoelectrical strike at site 20 is oriented N30W (Fig. 5), which is approximately perpendicular to the local strike of the valley and the surface geology. The valley is truncated to the west, so data polarized N60E at site 20 may be affected by that truncation. Previous modeling studies of 3-D structures have shown that the mode perpendicular to local strike can be interpreted with a 2-D model but that the parallel mode is likely affected by termination along structural strike (Wannamaker et al., 1984; Park, 1985). At site 20, the mode perpendicular to local strike is N30W. The TM (N30W) mode at site 20 is therefore included in our model of the N–S transect, but the TE (N60E) mode is not (Fig. 8). Additionally, we will include the component of the Hz transfer function oriented N–S at sites 8–9 and N30W at site 20 (Figs. 5 and 7).

Inversion of data from sites 1–9 and site 20 was performed using a regularized inversion algorithm (Mackie and Madden, 1993; Rodi and Mackie, submitted for publication) that minimized the sum of the χ^2 data misfit and the squared Laplacian of the deviation of the model from an apriori one. One of us (Mackie) modified this code to allow topography in the model and use of the Hz transfer function in the inversion. The actual model

spanned beyond the range of the data but we will show only a subset of it; see Park and Mackie (1997) for details. Error floors of 2.5% for the complex impedance (0.025 radians in phase and 5% in apparent resistivity) and 5% for the tipper transfer functions were used in the inversion to offset the influence of data values with unrealistically low error estimates. This floor was determined from scatter between adjacent points on the sounding curves and was relaxed to 10% for the TE mode after initial models had difficulty fitting both the TE and TM data. The apriori model used
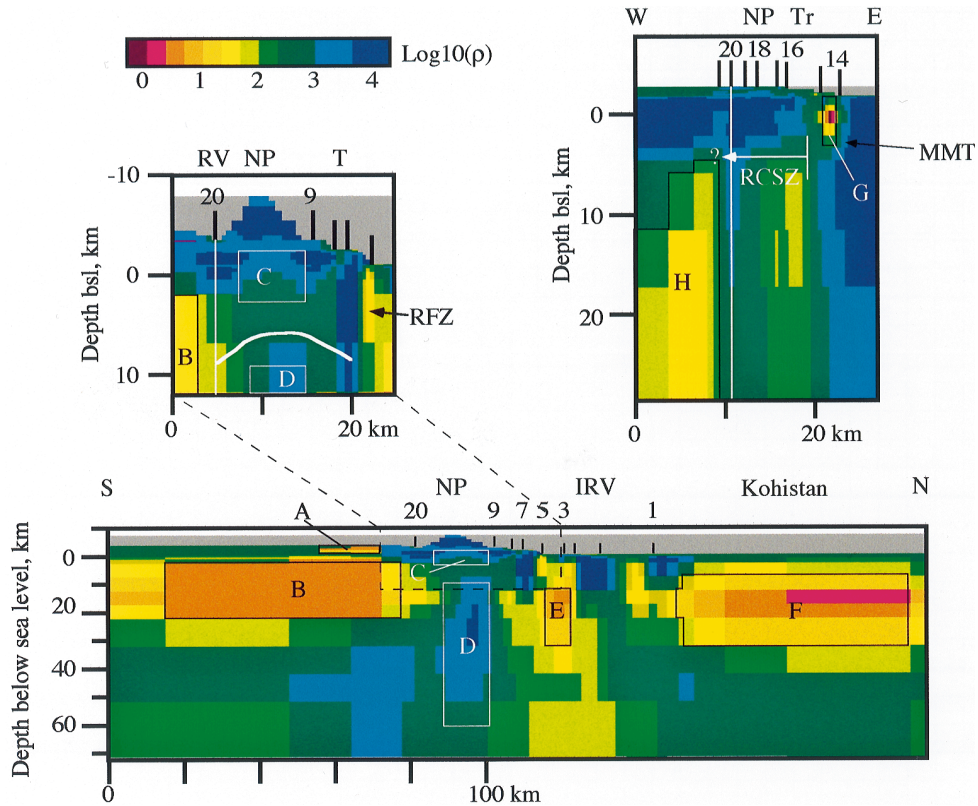
PLATE I. Resistivity models for the N–S and E–W transects shown in Fig. 1. Depths below sea level (bsl) are shown. For comparison, an expanded section of the N–S transect is plotted at the same vertical scale and exaggeration (1:1) as the E–W model. The heavy white line at depths of 5–8 km bsl on this expanded section is the inferred brittle–ductile transition inferred from seismicity (from Meltzer, et al., 1998). The dashed line on the N–S model outlines the expanded region. Regions A–H outlined in the models with solid lines are used for the sensitivity tests discussed in the text. The vertical white lines in expanded N–S section and the E–W section indicate the line of intersection between the two sections. Symbols used here are: IRV, Indus River valley; MMT, Main Mantle Thrust; NP, Nanga Parbat; RCSZ, Rupal Chichi shear zone; RV, Rupal valley; T, Tato; and Tr, Tarshing.

for this inversion was a layered half space with 500 ohm-m for depths shallower than 20 km bsl and 100 ohm-m below that.

The principal change from model presented in Park and Mackie (1997) is that the good conductor south of Nanga Parbat has moved to the south of Rupal Valley and the southernmost extent of data along the profile (Plate I). This is a robust result; induction arrows at sites 18–21 all indicate the presence of a good conductor to the south of Rupal Valley (Fig. 5). The excess conductivity to the south has also been modified to fit the variation of the transfer function with period (Fig. 8). The final model in Plate I fit the data with an overall rms misfit of 2.33. We will discuss fits to individual

sites in the next section, but most sites were fit with rms errors of less than 2.0 (Fig. 8). Larger misfits were found at sites 5 and 7 where the Raikot fault had a substantial influence on the E–W mode (Fig. 8). Additionally, several sites had responses for which the minimum phase relationship between the apparent resistivities and phases were violated (Fig. 9).

4.2. E–W transect

The N–S model in Plate I has two substantial conductive zones to the south of site 20 (zones A and B). How will those zones affect data recorded along the E–W profile? In other words, which
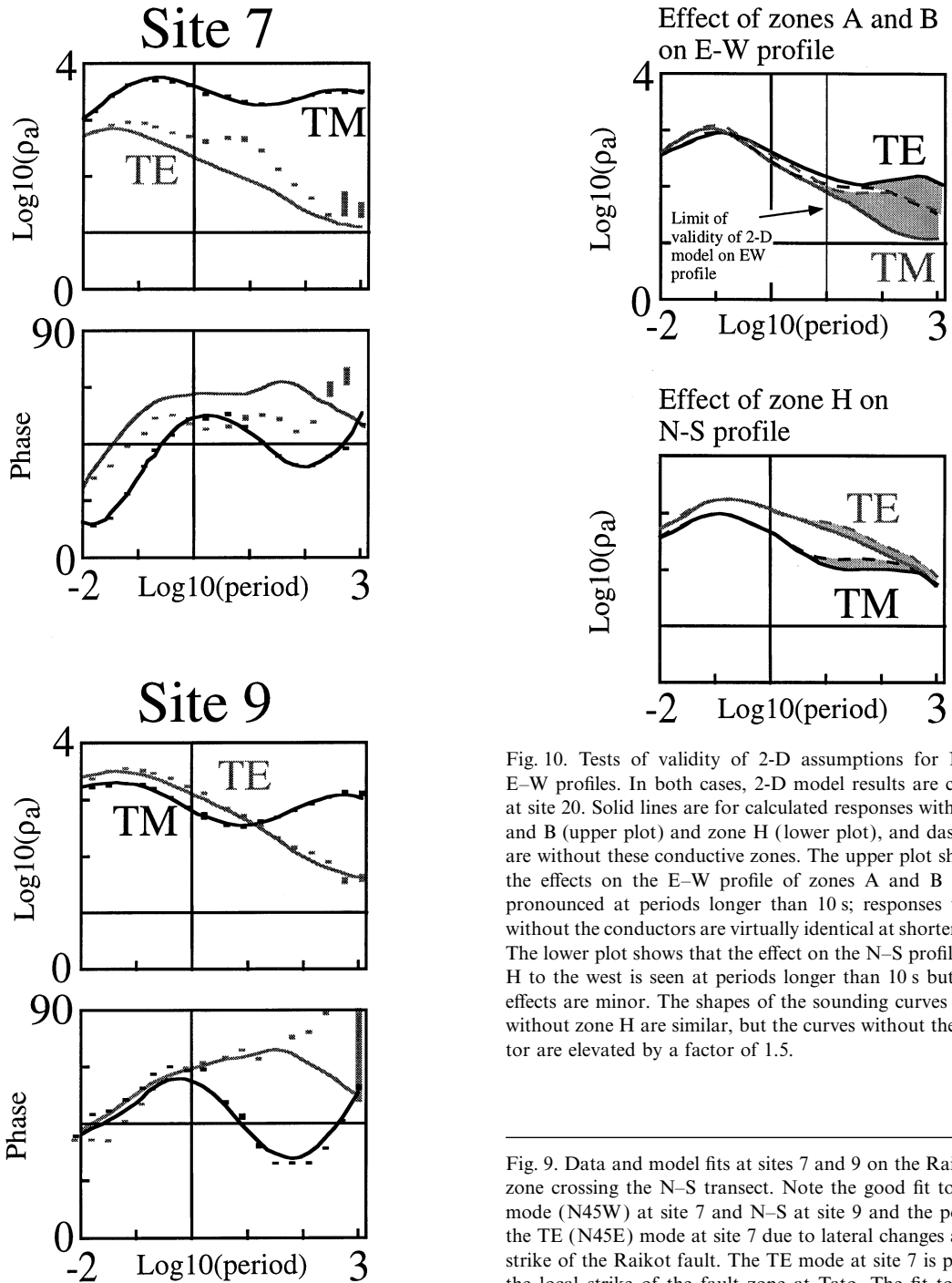
Fig. 10. Tests of validity of 2-D assumptions for N–S and E–W profiles. In both cases, 2-D model results are compared at site 20. Solid lines are for calculated responses with zones A and B (upper plot) and zone H (lower plot), and dashed lines are without these conductive zones. The upper plot shows that the effects on the E–W profile of zones A and B are most pronounced at periods longer than 10 s; responses with and without the conductors are virtually identical at shorter periods. The lower plot shows that the effect on the N–S profile of zone H to the west is seen at periods longer than 10 s but that the effects are minor. The shapes of the sounding curves with and without zone H are similar, but the curves without the conductor are elevated by a factor of 1.5.

Fig. 9. Data and model fits at sites 7 and 9 on the Raikot fault zone crossing the N–S transect. Note the good fit to the TM mode (N45W) at site 7 and N–S at site 9 and the poor fit to the TE (N45E) mode at site 7 due to lateral changes along the strike of the Raikot fault. The TE mode at site 7 is parallel to the local strike of the fault zone at Tato. The fit to the TM (N–S) mode at site 9 is much better because it lies outside the Raikot fault zone, although the TM phase at periods longer than 100 s is not the minimum phase. See Fig. 4 caption for plotting conventions.

modes and frequencies at sites 14–21 are relatively unaffected by these zones and can be fit solely with an E–W cross-section with a N–S structural strike? A comparison of computed responses from the N–S model at site 20 with and without zones A and B reveals that both modes at periods longer than 8 s are influenced those conductive zones (Fig. 10). We thus conclude that a 2-D model of the structure along the E–W transect will not be affected by conductors to the south if it is based on apparent resistivities and phases for both modes at periods less than 8 s. Additionally, the Hz transfer function (not shown) is affected appreciably at all periods greater than 0.07 s, so no transfer functions can be included in an E–W 2-D model. The dominant orientation of the transfer function at site 14 is E–W and not N–S, as we would expect if the response is due to the southern conductor, however. Therefore, the transfer function at site 14 was included in the 2-D inversion of the E–W transect. Phases from site 15 for the TE (N30W) mode were also excluded from the inversion because they violated the minimum phase assumption, presumably caused by mode mixing within the shear zone (Fig. 11).

An E–W model which fit the apparent resistivities and phases at sites 14–21 and the Hz transfer function at site 14 (Plate I) resulted in an overall rms misfit of 1.17. We show the model to depths of 28 km bsl only because a sensitivity analysis showed that this was the maximum depth of penetration for periods of 8 s or less. Misfits were low at most sites except sites 14 and 15. The rms misfit of 1.55 at site 15 was probably due to the inability of a 2-D model to completely capture the response of the southern boundary of the RCSZ (Fig. 11). The rms misfit of 1.89 at site 14 resulted from an inability to match the TE (N30W) mode and Hz transfer function simultaneously (Fig. 12). This model revealed a small, very conductive zone between sites 14 and 15 (zone G; Plate I) and a larger slightly conductive zone to the west of site 21 (zone H; Plate I).

4.3. Validity of the 2-D assumption on the N–S transect

How do the two conductive zones found crossing the E–W profile affect the data we used on the
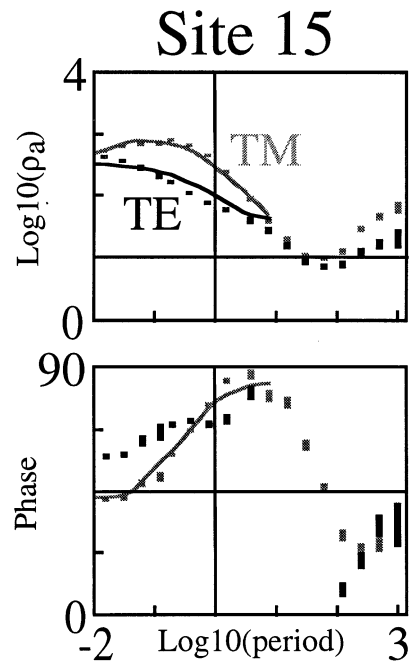

Fig. 11. Computed fits from E–W model at site 15. See caption of Fig. 4 for explanation. Note the non-minimum phase behavior of the TE (N30W) phase at the southern boundary of the RCSZ shear zone. Data at periods less than 8 s only were fit with the model. See Fig. 4 caption for plotting convention.

N–S profile? The model derived for the N–S profile did not include the effects of zones G and H, and we need to reexamine our assumptions in light of the structure on the E–W profile. We assess the influence of zones G and H by comparing responses at site 20 with and without these two zones (Fig. 10). Removal of zone G results in only 10–20% changes in apparent resistivities and 2–3° in phases for the TM (N30W) mode, and these changes are not shown here. The TE (N60E) mode is virtually unaffected by the smaller conductor. Removing the larger, western conductor (zone H) increases the apparent resistivities in the TM (N30W or N–S) mode by as much as a factor of 50% at a period of 30 s and the phase by as much as 5° at periods longer than 1 s (Fig. 10). This would mean that a model based on this mode may overestimate actual resistivities by a factor of 1.5 or so because the effect of the western conductor was not included in that model. Because the model of the N–S profile already has very resistive rocks
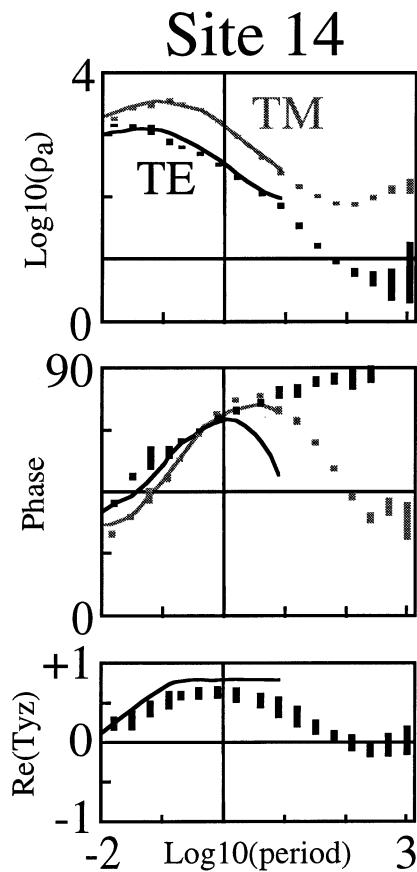
Site 14

Fig. 12. Computed fits from E–W model at site 14. See caption of Fig. 4 for explanation. This best-fit model was unable to simultaneously match the TE (N–S) mode phases and the Hz transfer function (Tyz). See Fig. 4 caption for plotting convention.

fied versions of the 2-D cross-sections in Plate I and computed responses with and without zones B, F, and H (Plate I). Again, we will examine the responses at site 20 only.

Comparison of responses with and without zone H shows that the TM (N–S) mode is increased by a maximum factor of 2.5 at 30 s periods (Fig. 13), which is only slightly larger than the factor of 1.5 estimated from Fig. 10. The TE (E–W) mode is virtually unaffected. Therefore, our conclusion from Fig. 10 that resistivities may be overestimated in a 2-D model of the N–S profile is still valid. Comparison of responses with and without zones B and F shows that data at periods less than 8 s are unaffected by these zones (Fig. 13). Therefore, basing the E–W profile on data recorded at periods less than 8 s will yield a valid 2-D model. This was also the conclusion from Fig. 10. Note that the differences in the responses in Figs. 10 and 13 are due to the fact that the former is based on the exact 2-D model that fit the data, while the latter is necessarily a simplified version of the models in Plate I.

We have now produced 2-D models of the geoelectrical structure along the N–S and E–W transects and have shown that the effects of the conductors identified on one profile should not significantly affect the model derived for the other. Where the models cross at site 20, there is a reasonably good agreement (Plate I). Both profiles have rocks with resistivities greater than 1000 ohm-m to depths of 2–4 km bsl and less resistive values beneath. The next step is to determine bounds that can be placed on important features in both models.

5. Sensitivity analysis

5.1. N–S transect

The most surprising result in Plate I is the presence of very resistive rocks beneath the higher elevations between sites 9 and 20 to depths of at least 50 km bsl. Given the abundant geological and surficial evidence for fluids, we would have expected to find conductive rocks in this region. What limits can be placed on the resistivities in this region, especially considering that there are

in the vicinity of site 20 (Plate I), we conclude that potential errors introduced through the use a 2-D model along the N–S transect will not affect our interpretation appreciably. Reduction of the high resistivities beneath Nanga Parbat in order to account for conductive zone H would still leave extremely high values in the rapidly exhuming region.

We have so far used 2-D models to assess the effects of structure off the axis of the N–S and E–W profiles, but are those models valid? The structure is really 3-D, and would a 3-D model of the structure yield results different from those in Fig. 10? We constructed a 3-D model from simpli-
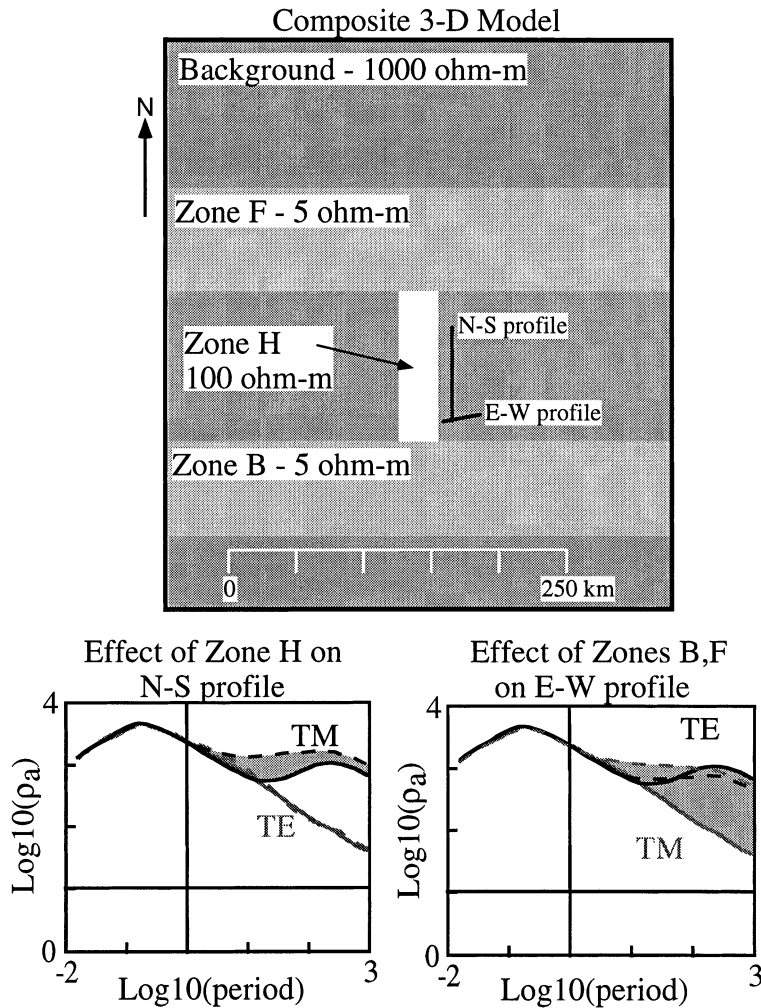
Fig. 13. Composite 3-D model constructed from simplified versions of cross-sections in Plate I. This model contains the Indus River valley from Fig. 6 (not shown) as well as zones B, F, and H at depths of 2–22 km bsl (slice at 12 km is pictured). Responses at site 20 are shown as solid lines in both apparent resistivity plots. The effect of removing zone H from the pictured model is shown on the left (dashed lines) and consists of raising the TM (N–S) mode by a maximum factor of 2.5 at 30 s. The TE (E–W) mode is unaffected. Removal of zones B and F and the extension of zone H to the north and south to approximate a 2-D model crossing the E–W profile is shown on the right (dashed lines). Both modes are affected, although the TM (E–W) mode is offset by an order of magnitude. This latter test confirms that data at periods longer than 8 s are affected by the conductor parallel to and south of the E–W profile. See Fig. 4 caption for plotting convention.

no soundings that overlie it directly? We follow the methodology of Park et al. (1996) to assess these limits. The inversion is fundamentally ill-posed and non-unique. Simply replacing the resistive rocks with more conductive rocks and showing that the computed responses differ is insufficient; there may be alternative models with those more conductive rocks that fit the data just as well. We instead constrain the region of interest and allow the 2-D inversion to find its best-fitting alternative model. Examination of the fits to the data reveal whether the alternative model is as good. Bounds are then determined from the range of alternative models that fit the data to within the errors.
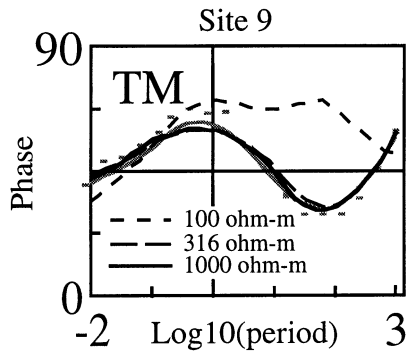
Fig. 14. Sensitivity of the TM (N–S) mode phase at site 9 to zone D in Plate I. The observed data and the response from the best fitting model are shown here and in subsequent sensitivity tests with gray error bars and the gray line, respectively. Note how the model with a fixed resistivity of 1000 ohm-m at depths of 10–60 bsl beneath Nanga Parbat most closely matches the data (solid black line). See Fig. 4 caption for plotting convention.

Resistivities beneath the peak at depths of 10–60 km bsl were constrained to values of 100, 316, and 1000 ohm-m (zone D; Plate I) and the inversions run. The TM (N–S) phases (and apparent resistivities) at site 9 showed the largest fluctuations at any site (Fig. 14). While the variations between models are small, the calculated phases lie outside the error bounds of the data for all but the most resistive models. In other words, the inversion was unable to find an alternate model that fit the data as well as did our preferred model. If the trend in Fig. 14 is extrapolated, the resistivity values in our best-fitting model (Plate I) are still probably underestimated. We can conclude from this comparison that a minimum average resistivity of 1000 ohm-m in zone D is necessary to fit the data.

Resistivities beneath the peak at depths of 2 km above sea level (asl) to 3 km bsl were constrained in a second test (zone C; Plate I). Values of 100, 316, and 1000 ohm-m were again used. The TE (E–W) mode at site 9 exhibited the greatest sensitivity to this zone (Fig. 15). This test also shows that a minimum average resistivity of 1000 ohm-m is needed to fit these data, and values over 10 000 ohm-m in our best fitting model are preferred.

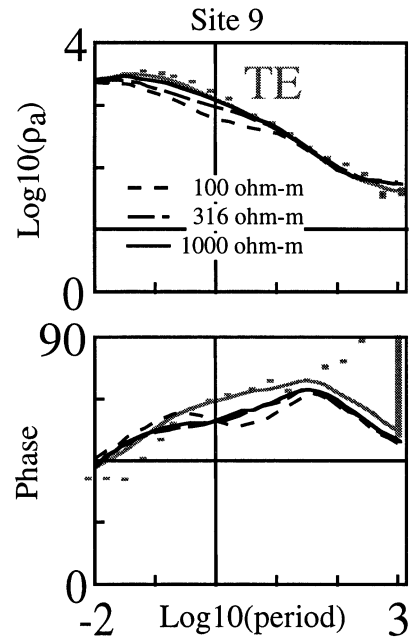Both of these tests show that average resistivities beneath the most rapidly exhuming section of

Fig. 15. Sensitivity of the TE (E–W) mode apparent resistivity and phase at site 9 to zone C in Plate I. Note how a model with a fixed resistivity of 1000 ohm-m in this shallow region beneath Nanga Parbat provides the best match to the data (solid black line). See Fig. 4 caption for plotting convention.

Nanga Parbat must exceed 1000 ohm-m, but could the fluids mentioned in Section 1 be distributed locally in fault zones and not contribute to the bulk resistivity of the rocks? This model and the model in Park and Mackie (1997) show that the Raikot fault is conductive to depths of 10 km bsl (the conductive zone E in Plate I is not needed to fit any of the data). Is it possible that another fault zone like the Raikot fault is present and simply missed by the sparse station spacing across the high elevations? In order to answer this question, we embedded a conductive body 5680 m wide and 4000 m thick at an elevation of 2 km asl between sites 9 and 20. Varying this body's resistivity between 10 and 100 ohm-m had little effect on apparent resistivities and phases but produced significant variations in the Hz transfer function at site 20 (Fig. 16). Any resistivity greater than 100 ohm-m would result in an acceptable fit to the existing data.

While geometry will play some role in this response, the important factor for the Hz transfer
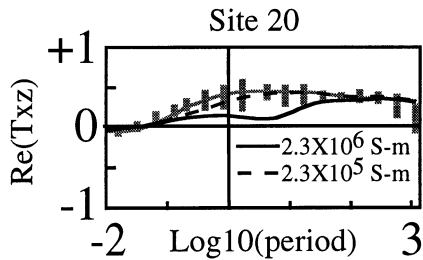
Fig. 16. Sensitivity of the Hz transfer function at site 20 to isolated conductors beneath Nanga Parbat. An areal conductance of 2.3×10^5 S·m provides an acceptable match to the data. See Fig. 4 caption for plotting convention.
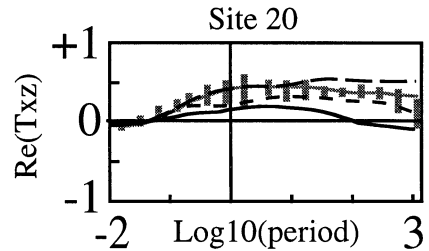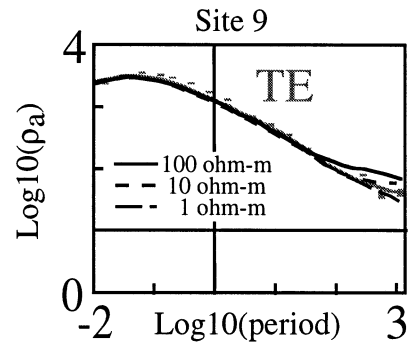

Fig. 17. Sensitivity of the TE (E–W) mode apparent resistivity at site 9 and the Hz transfer function at site 20 to zones A and B in Plate I. Models with fixed resistivities in these zones of 1 and 10 ohm-m bracket the observed responses. See Fig. 4 for plotting convention.

function is the areal conductance (length × width/resistivity). When the areal conductance of this isolated body was 2.3×10^6 S·m, it affected the Hz transfer function at site 20. Reduction of the areal conductance to 2.3×10^5 S·m yields an acceptable Hz response. We therefore conclude that isolated bodies with cumulative areal conductances of less than 2.3×10^5 S·m could be present beneath Nanga Parbat. Assuming a resistivity similar to that of the Raikot fault (i.e. 10 ohm-m), conductive zones with a maximum cross-section of 1500 m × 1500 m could be found in this region. In comparison, the Raikot fault zone has an areal conductance of 9.8×10^6 S·m (or 40 times more conductive than the maximum permissible body beneath Nanga Parbat).

One of the counterintuitive (and therefore suspect) results in Plate I is the presence of substantial conductive bodies to the north and south of the MT profile. With no data there, can we be certain that these exist? Furthermore, the region to the south does not simply show one body. It instead has two good conductors, one shallow and one deep (zones A and B; Plate I). We will show through sensitivity tests that these bodies are necessary to fit the data.

Zones A and B in Plate I were constrained to values of 1, 10, and 100 ohm-m. The observed data were fit best with the most conductive value (1 ohm-m) but all three tests resulted in acceptable fits because the inversion placed more conductive material around the periphery of the constrained regions. A second set of trials were then run, and all structure beyond 5 km south of site 20 was

constrained. Those results showed that the Hz transfer function at site 20 and the TE (E–W) apparent resistivity at site 9 could not be fit with average resistivities greater than 10 ohm-m (Fig. 17). A value of 1 ohm-m was too conductive, leading to a preferred average resistivity of 3 ohm-m.

An additional round of tests assessed the need for the deep conductor to the south (Zone B). Unacceptable fits to the TM (N–S) phases at sites 9 and 20 and the Hz transfer function at site 20 (Fig. 18) resulted from resistivities greater than 10 ohm-m for the deep conductor. Changes in the Hz transfer function (Txz) were seen at site 20 for periods longer than 40 s only; the response at shorter periods is due to the shallower conductor (Zone A). We conclude from these tests that our data are sensitive to structure to the south of the profile. While there are certainly other possible geometries for the conductors found, bounds can be placed on their areal conductances, and we
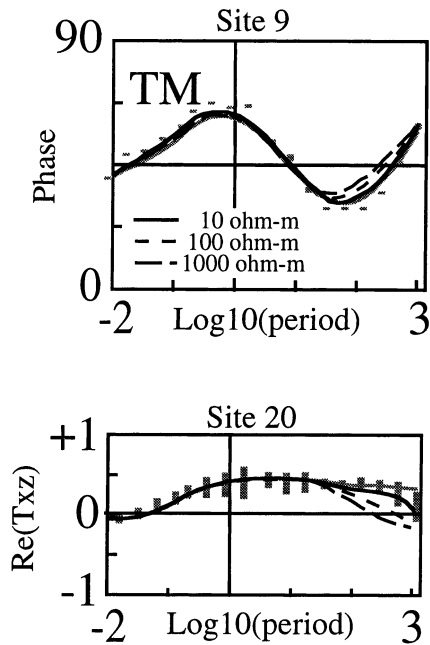
Fig. 18. Sensitivity of the TM (N–S) mode apparent resistivity at site 9 and the Hz transfer function at site 20 to zone B in Plate I. Models with fixed resistivities of less than 10 ohm-m provide acceptable fits. See Fig. 4 caption for plotting convention.
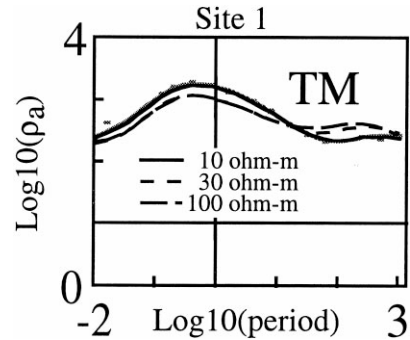

Fig. 19. Sensitivity of the TM (N–S) mode apparent resistivity at site 1 to zone F in Plate I. Values of less than 10 ohm-m to the north of site 1 are permissible. See Fig. 4 caption for plotting convention.

profile are required to fit the data along the profile. We will discuss the bounds further when we consider the geological implications of these results.

5.2. E–W transect

The most prominent feature of the E–W model in Plate I is the good conductor located between sites 14 and 15 at an elevation of 1 km bsl (zone G). Sensitivity tests show that the TE (N30W) mode apparent resistivities and phases are best fit with an average resistivity of 2 ohm-m in this region (Fig. 20). The limited vertical extent of this conductor is constrained by the limited periods for which its effect is seen. This test also illustrates the contradictory nature of the Hz transfer function and the TE (N30W) mode apparent resistivities and phases. The Hz transfer function (Tyz) is fit better with an average resistivity of 100 ohm-m, but the apparent resistivities are badly misfit (Fig. 20). As the resistivity of this body is decreased, the apparent resistivities are fit increasingly better but at the expense of a poorer Hz fit. The eastern edge of this profile crosses the MMT back onto the Kohistan terrane (Fig. 5), and this site is likely experiencing the competing effects of the shear zone in the Indian crust and this terrane.

The other notable feature of the E–W model is the moderately conductive region to the west of site 21 (zone H; Plate I). Tests show that the TM (N60E) mode apparent resistivities and phases are affected moderately by the resistivity of this region

have some constraints on their distribution. A minimum cumulative areal conductance of 1.2×10^8 S·m is needed, and this must be distributed with some of the conductance in the upper 5 km of the section. The preferred model has an areal conductance of 4.0×10^8 S·m, but a value this high is not required. Note that the minimum value is only 12 times more conductive than the Raikot fault, where our data do provide good constraints. We conclude that this areal conductance, although large, is not unreasonable.

Similar tests on the conductor north of site 1 (zone F; Plate I) show that this, too, is required. The TM (N–S) mode apparent resistivities and phases require a maximum resistivity of 10 ohm-m in the northern conductor (Fig. 19), and a minimum cross-sectional conductance of 8.0×10^7 S·m is required. This is approximately eight times more conductive than the Raikot fault. From both of these tests, we conclude that the conductors shown in Plate I to the north and south of the MT
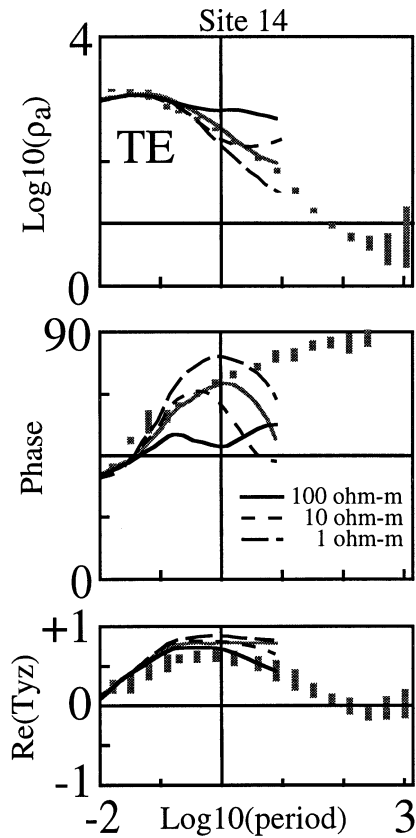
Fig. 20. Sensitivity of the TE (N–S) mode apparent resistivity and phase and the Hz transfer function at site 14 on the E–W transect to zone G in Plate I. Note how decreasing the resistivity of this zone worsens the fit to the transfer function but improves the fit to the phase and apparent resistivity. See Fig. 4 caption for plotting convention.

(Fig. 21). However, any value less than 100 ohm-m results in an acceptable fit to the data. We conclude that both the good conductor between sites 14 and 15 and the moderate conductor to the west of site 21 are robust features of this model.

6. Discussion

Our principal result is that there is no evidence of widespread conductors to depths of 50 km bsl beneath the highest elevations of Nanga Parbat and the rapidly exhuming region to the north. Average resistivities in this region exceed 1000 ohm-m, and only a few isolated conductors
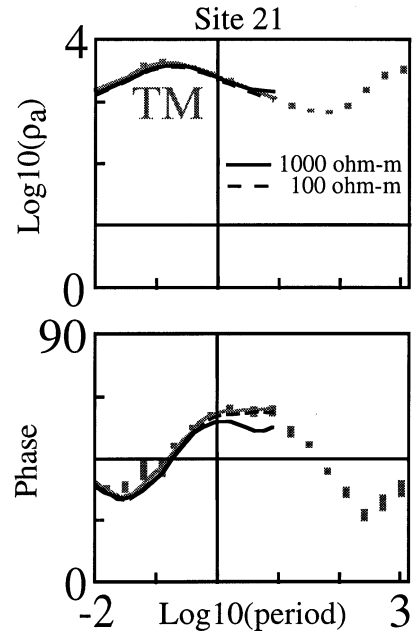

Fig. 21. Sensitivity of the TM (N60E) mode apparent resistivity and phase to zone H in Plate I. A resistivity less than 100 ohm-m for the western conductor results in an acceptable fit to the data. See Fig. 4 caption for plotting convention.

are permitted by the Hz data. The high resistivities span depths both above and below the brittle–ductile transition, as determined by the cessation of seismicity beneath Nanga Parbat (Meltzer et al., 1998), and no discernible change in resistivity is seen at that transition (Plate I). We assume that there is an interconnected conducting phase beneath Nanga Parbat because the rock resistivity is indeed finite and because silicate minerals at the pressures and temperatures in the crust are far more resistive. Possible candidates for this phase are partial melt, graphite, and aqueous brines (it is unlikely that there are basaltic melts beneath Nanga Parbat). A less likely candidate is a metallic phase such as sulfides or oxides. Given the abundant evidence for shallow fluids beneath Nanga Parbat, we will first calculate the fraction of interconnected fluid needed to account for a resistivity of 1000 ohm-m. The rock resistivity is related to fluid resistivity and fluid fraction (f): $\rho_{rock} = \rho_{fluid}/f^n$ where $n \approx 1$ for partial melts and interconnected networks. Nesbitt (1993) has shown that the resistivity of a 3.5 wt% salt solution

at pressures of 3 kbar and temperatures of 300–500°C is approximately 0.04 ohm-m. Based on the salt content and temperatures of fluid inclusions at Nanga Parbat (Craw et al., 1994), this is a reasonable estimate for fluid resistivity there. With minimum rock resistivities of 1000 ohm-m, the maximum interconnected fluid fraction is 0.004% (40 ppm). Note that the resistivity of graphite is even lower (10^{-5} ohm-m), so the fraction of interconnected graphite could be no larger than 0.01 ppm. The MT data therefore indicate that there is a very small fraction of interconnected aqueous fluid phase in the rocks beneath Nanga Parbat. Seemingly contradictory evidence for abundant shallow aqueous fluids is reviewed in the Section 1, however. How can these observations be reconciled?

We separate this discussion into regions above and below the brittle–ductile transition (Fig. 22). Several independent lines of evidence locate this boundary at a depth of 5–8 km bsl and temperatures of 400–450°C beneath Nanga Parbat. Meltzer et al. (1998) show that abundant local seismicity ceases abruptly at depths of 5 km bsl beneath the rapidly exhuming region and at depths
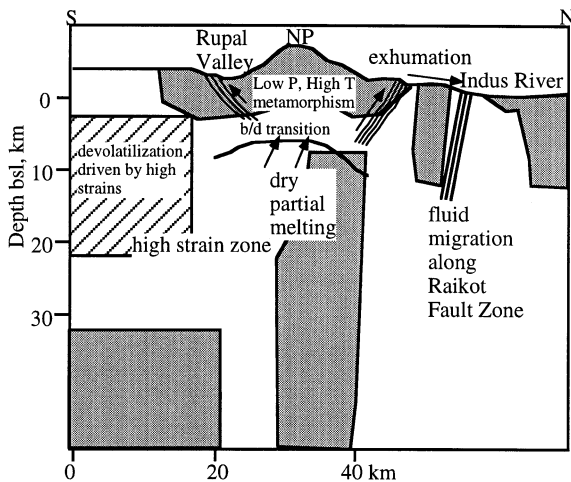

Fig. 22. Interpretive geologic cross-section (after Zeitler and Koons, 1998) overlaid on segment of N–S resistivity section from Plate I. Shaded areas are resistivities greater than 1000 ohm-m, and diagonal lines denote regions with resistivities less than 3 ohm-m. Only robust features of the model are shown. Arrows show advection of crust and other mass movement (faults, erosion).

of 8 km bsl on the flanks. Fluid inclusions from brittly deformed quartz veins equilibrated at 400°C, while those from ductily deformed veins equilibrated at 450°C (Craw et al., 1997). High $\delta^{18}O$ values in the granites and low values in adjacent migmatites have led Chamberlain et al. (1995) to propose a dual hydrothermal system with a shallow meteoric system and a deeper system with magmatic or metamorphic fluids. Most of the fluid inclusions are associated with the shallow circulation system above the brittle–ductile transition (Craw et al., 1994, 1997). Within this zone, the fluid inclusions show a vapor-dominated geothermal system. The presence of aqueous vapor is consistent with the high resistivities and low content of interconnected brines; rocks in a dry steam system (Craw et al., 1997) should be resistive. Recharge of this system by downward circulation of meteoric water probably occurs along portions of the Raikot fault at the base of the steepest continuous topographic gradient (7 km elevation loss over approximately 28 km; Fig. 22) in the world. We cannot exclude the possibility that other recharge zones (or fluid-filled fractures) are present between sites 9 and 20 at Nanga Parbat, but they must represent a small fraction of the volume based on our sensitivity studies.

Below the brittle–ductile transition, we would normally expect to find aqueous brines associated with metamorphic and/or magmatic processes. Hydration reactions associated with heating of the crustal rocks can result in brines with as much as 10 wt% NaCl, but fluid volumes will likely be much less than 1% (Walther, 1994). At Nanga Parbat, the rocks being reheated are old gneisses of the Indian crust and were likely dehydrated in earlier metamorphic events that created them. Thus, there may be little aqueous fluid available under any conditions. Koons (Koons, 1998) model of strain at Nanga Parbat (Koons, 1998) shows rapid advection of rock through the brittle–ductile transition. This active deformation should enhance the wetting characteristics of the brines on the feldspars (Tullis et al., 1996) and pyroxenes (Watson and Lupulescu, 1993). Thus, any aqueous brines present below the brittle–ductile transition would likely be interconnected, and our estimate

of 0.004% therefore represents an upper bound for this region. Note that higher bulk fluid fractions are possible if the fluids are CO_2-rich because such fluids are resistive.

One of the initial questions posed at Nanga Parbat was whether partial melting occurred due to rapid decompression of water-undersaturated continental crust or because of fluxing of hot, shallow rocks by metamorphic fluids from deeper levels. Given that young granites are present, partial melting is surely occurring. Can the resistivity be used to estimate how much partial melt is generated and under what conditions? One complication is that the resistivity of granitic melts depends critically on water content, and it ranges from values as low as 0.1 ohm-m for water-saturated melts to as high as 1000 ohm-m for vapor-absent melts (Wannamaker, 1986). Further, the resistivity of the melt can actually increase under conditions of continued undersaturated melting because the water in the melt becomes more diluted. Given this range of possible resistivities for melt beneath Nanga Parbat, we cannot estimate uniquely the amount of partial melt beneath the brittle–ductile transition. The high resistivity of these rocks does permit certain conclusions, however. If wet partial melting were occurring, then the granitic melt would have an estimated resistivity of 0.3 ohm-m (Wannamaker, 1986). If this melt were interconnected, then the region beneath Nanga Parbat could contain no more than 0.003% partial melt in order to match the observed bulk resistivity of the rock. Higher fractions of partial melt could be present if undersaturated partial melting were occurring; granitic melts formed under these conditions can be as resistive as the surrounding rock. Because we have resistive rocks below the brittle–ductile transition and because partial melting is certainly occurring, we must conclude that it occurs under water-undersaturated conditions. The granites are formed by partial melting of 'dry' continental crust caused by decompression as that crust is advected upward (Fig. 22).

This partial melting is not widespread, however. Preliminary seismic tomographic results show that *Vp* and *Vs* values beneath Nanga Parbat velocities, while lower than normal, are still too high for a large, shallow magma body (Meltzer, et al., 1998).

Prominent shear wave arrivals are seen throughout the region, although there is evidence of scattering that could be indicative of small partial melt zones. Additionally, the young granitic bodies are not widespread but instead appear to be concentrated along shear zones (Schneider et al., 1999). Schneider et al. (1999) have proposed that a small amount of melt is produced by decompression melting and that melt migrates to the shear zones. In summary, the MT data are consistent with the presence of small bodies of granitic melt formed by decompression melting of water-undersaturated continental crust.

While the resistive rocks beneath Nanga Parbat were the most surprising result of this study, several distinctive conductive regions were identified on the N–S and E–W transects. The most obvious of these are the two conductive regions south of site 20 (Plate I). The shallow conductor required south of the profile is probably associated with structures in the ductile southern boundary of the Rupal-Chichi shear zone (RCSZ) (Schneider et al., 1999). Where our E–W MT profile crosses this boundary between sites 15–17 (Fig. 2), we see generally lower resistivities at depths below sea level. Field evidence for hydro-thermal alteration is observed on brittle faults in the part of the shear zone in central Rupal Valley (between sites 14 and 15), certainly indicating fluid circulation. These fluids and the clay alteration products observed at this location could be the cause of the prominent localized conductor between sites 14 and 15.

The deeper conductor to the south may be related to metamorphism of lower grade schists south of Rupal Valley (Fig. 22) or to disseminated graphite in the Sakhala formation (Smith et al., 1992). While neither of these rock types is found at the surface, both are found elsewhere in the region and may be present at depth. The low resistivity of this body (3 ohm-m) could result from either 0.003% disseminated graphite or $\sim$1% of 3.5 wt% NaCl brine. Fluids could also facilitate melting of the continental crust south of Nanga Parbat; young (NPHM-age) biotite-rich granites are localized in the western marginal shear zone of the Nanga Parbat massif and at the southern edge of the RCSZ (Fig. 2). Koons (1998) has

proposed a model whereby Indian crust is advected northeastward and upward into the syntaxis, and it experiences deformation-induced heating and metamorphism (Fig. 22). These prograde metamorphic reactions liberate the brines to which we attribute this southern, deeper conductor. Dry gneisses then continue advecting northeastward and rise rapidly in the vicinity of Nanga Parbat, which results in 'dry' partial melting to form the granites. Such a model simultaneously explains the good conductors to the south of site 20 and the extremely resistive rocks beneath the rapidly exhuming portion of the massif.

The midcrustal conductive region to the north in the Kohistan crust (zone F; Plate I) is reminiscent of midcrustal conductors seen elsewhere in continental crust. While a minimum cross-sectional conductance has been computed for this body, there are no constraints on its northward extension. If it is instead the southern edge of a laterally extensive midcrustal conductor, then we can compare its vertical conductance (thickness/resistivity) to that of continental crust elsewhere. Its vertical conductance is 1500 S, which is much higher than seen for old continental crust (Haak and Hutton, 1986) but not unreasonable for crust in active margins. This high a conductance is similar to that seen along the INDEPTH profile in Tibet (Leshou, et al., 1996). Normally, the brittle–ductile transition traps upward-migrating aqueous fluids beneath it in active tectonic regions (Bailey, 1990); this is the likely explanation for the crustal conductivity profile in Kohistan. At Nanga Parbat, any fluid generated escapes rapidly through the brittle–ductile transition because of the active exhumation of the NPHM.

References

Bailey, R.C., 1990. Trapping of aqueous fluids in the deep crust. Geophys. Res. Lett. 17, 1129–1132.

Chave, A.D., Thomson, D.J., Ander, M.E., 1987. On the robust estimation of power spectra, coherences, and transfer functions. J. Geophys. Res. 92, 633–648.

Chamberlain, C.P., Zeitler, P.K., Barnett, D.E., Winslow, D., Poulson, S.R., Leahy, T., Hammer, J.E., 1995. Active hydrothermal systems during recent uplift of Nanga Parbat, Pakistan Himalaya. J. Geophys. Res. 100, 439–453.

Craw, D., Koons, K.O., Winslow, D., Chamberlain, C.P., Zeitler, P.K., 1994. Boiling fluids in a region of rapid uplift, Nanga Parbat Massif, Pakistan. Earth Planet. Sci. Lett. 128, 169–182.

Craw, D., Chamberlain, C.P., Zeitler, P.K., Koons, P.O., 1997. Geochemistry of a dry steam geothermal zone formed during rapid uplift of Nanga Parbat, northern Pakistan. Chem. Geol. 142, 11–22.

Groom, R.W., Bailey, R.C., 1989. Decomposition of magnetotelluric impedance tensors in the presence of local three-dimensional galvanic distortion. J. Geophys. Res. 94, 1913–1925.

Haak, V., Hutton, R., 1986. Electrical resistivity of the continental lower crust. In: Dawson, J.B., Carswell, D.A., Hall, J., Wedepohl, K.H. (Eds.), The Nature of the Lower Continental Crust. Geological Society, London, pp. 35–49.

Hirasuna, B., Park, S.K., 1993. Correction of magnetotelluric data influenced by static shift: a comparison of methods. EOS Trans. Am. Geophys. Union 74, 230.

Jones, A.G., 1992. Electrical conductivity of the continental lower crust. In: Fountain, D.M., Arculus, R.J., Kay, R.W. (Eds.), Continental Lower Crust. Elsevier, New York, pp. 81–143.

Koons, P., 1998. Big mountains, big rivers and hot rocks: beyond isostasy. EOS Trans. Am. Geophys. Union 79 Suppl., F908.

Larsen, J.C., Mackie, R.L., Manzella, A., Fiordelisi, A., Rieven, S., 1996. Robust smooth magnetotelluric transfer functions. Geophys. J. Int. 124, 801–819.

Leshou, C., Booker, J.R., Jones, A.G., Wu, N., Unsworth, M.J., Wenbo, W., Handong, T., 1996. Electrically conductive crust in southern Tibet from INDEPTH magnetotelluric surveying. Science 274, 1694–1696.

Mackie, R.L., Madden, T.R., 1993. Three-dimensional magne-
    totelluric inversion using conjugate gradients. Geophys.
    J. Int. 115, 215–229.
Mackie, R.L., Madden, T.R., Park, S.K., 1996. A three-dimen-
    sional magnetotelluric investigation of the California Basin
    and Range. J. Geophys. Res. 101, 16221–16239.
Meltzer, A., Sarker, G., Seeber, L., Armbruster, J., 1998. Snap,
    crackle, pop! Seismicity and crustal structure at Nanga
    Parbat Pakistan Himalaya. EOS Trans. Am. Geophys.
    Union 79 Suppl., F909.
Nesbitt, B.E., 1993. Electrical resistivities of crustal fluids.
    J. Geophys. Res. 98, 4301–4310.
Park, S.K., 1985. Distortion of magnetotelluric sounding curves
    by three-dimensional structures. Geophysics 50, 785–797.
Park, S.K., Mackie, R.L., 1997. Crustal structure at Nanga
    Parbat, northern Pakistan, from magnetotelluric soundings.
    Geophys. Res. Lett. 19, 2415–2418.
Park, S.K., Torres-Verdin, C., 1988. A systematic approach to
    the interpretation of magnetotelluric data in volcanic envi-
    ronments with applications to the quest for magma in Long
    Valley, California. J. Geophys. Res. 93, 13265–13283.
Park, S.K., Hirasuna, B., Jiracek, G.R., Kinn, C.L., 1996. Mag-
    netotelluric evidence of lithospheric mantle thinning beneath
    the southern Sierra Nevada. J. Geophys. Res. 101,
    16241–16255.
Parkinson, W.D., 1962. The influence of continents and oceans
    on geomagnetic variations. Geophys. J. Roy. Astr. Soc. 6,
    441–449.
Rodi, W.L., Mackie, R.L., publication. Non-linear conjugate
    gradients algorithm for 2-D magnetotelluric inversion. Geo-
    physics. submitted for publication
Schneider, D., Edwards, M.A., Kidd, W.S.F., Asif Khan, M.,
    Seeber, L., Zeitler, P.K., 1999. Tectonics of Nanga Parbat,
    western Himalaya: Synkinematic plutonism within the
    doubly vergent shear zones of a crustal-scale pop-up struc-
    ture. Geology 27, 999–1002.

Smith, H.A., Chamberlain, C.P., Zeitler, P.K., 1992. Documen-
    tation of Neogene regional metamorphism in the Himalayas
    of Pakistan using U–Pb monazite. Earth Planet. Sci. Lett.
    113, 93–105.
Tullis, J., Yund, R., Farver, J., 1996. Deformation-enhanced
    fluid distribution in feldspar aggregates and implications for
    ductile shear zones. Geol 24, 63–66.
Vozoff, K., 1991. The magnetotelluric method. In: Nabighian,
    M.N. (Ed.), Electromagnetic Methods in Applied Geophys-
    ics. Society of Exploration Geophysicists, Tulsa, OK,
    pp. 641–711.
Walther, J.V., 1994. Fluid–rock reactions during metamorphism
    at mid-crustal conditions. J. Geol. 102, 559–570.
Wannamaker, P.E., 1986. Electrical conductivity of water-
    undersaturated crustal melting. J. Geophys. Res. 91,
    6321–6327.
Wannamaker, P.E., Hohmann, G.W., Ward, S.H., 1984. Mag-
    netotelluric responses of three-dimensional bodies in layered
    earths. Geophysics 49, 1517–1533.
Watson, E.B., Brenan, J.M., 1987. Fluids in the lithosphere, 1.
    Experimentally-determined wetting characteristics of
    CO_2–H_2O fluids and their implications for fluid transport
    hot rock physical properties and fluid inclusion formation.
    Earth. Planet. Sci. Lett. 85, 497–515.
Watson, E.B., Lupulescu, A., 1993. Aqueous fluid connectivity
    and chemical transport in clinopyroxene-rich rocks. Earth
    Planet. Sci. Lett. 117, 279–294.
Zeitler, P.K., 1985. Cooling history of the northwestern Hima-
    laya Pakistan. Tectonics 4, 127–151.
Zeitler, P.K., Chamberlain, C.P., Smith, H.A., 1993. Synchron-
    ous anatexis metamorphism and rapid denudation at Nanga
    Parbat (Pakistan Himalaya). Geology 21, 347–350.
Zeitler, P.K., Koons, P.O., 1998. Nanga Parbat as tectonic
    aneurysm: a metamorphic signature of indentor-corner
    dynamics. EOS Trans. Am. Geophys. Union 79 Suppl.,
    F910.